# X-RAY TOMOGRAPHY OF STRUCTURES IN CLAY GEOSYNTHETIC BARRIERS (CBR-C)

P. Schick
Haar, Germany

S. M. Schmitz
University of the Federal Armed Forces, Munich, Germany

ABSTRACT: In practical use Clay Geosynthetic Barriers (CBR-C) are subjected to different loads, the consequences of which cannot be calculated reliably with today's level of knowledge. Salt solution, moisture and temperature loads cannot be described in terms of soil mechanics only. In fact, clay mineralogical and chemical-thermodynamical effects have to be taken into account, too. Therefore, extensive measurements and description of these phenomena are of special importance. In this paper, the development of structures that may be identified with modern computerized x-ray tomography is described and quantified. The development of structures under defined extreme loads may strongly affect the desired sealing properties. The long-term objective is to model structure development processes in fine-grained soils in a basically physical and elementary way.

## 1 INTRODUCTION

Clay Geosynthetic Barriers (CBR-C) are frequently used in the areas of technical environmental protection (waste dump sealing systems, roads in water protection areas) and waterway construction (canal sealing). The most important factors to be considered here are the permeability coefficient, the chemical persistence of geotextile and bentonite and the behavior in the event of freeze alternating with thaw and of dehydration-humidification cycles [1]. The use of CBR-C is also largely influenced by the presence of coarse-grained protective covers and their correct set-up.

In the event of drying, the volume of highly plastic clays such as bentonite strongly decreases, which results in intensive crack formation. The adsorption-water films have a formative influence on the soil mechanical behavior. In order to describe the drying behavior, we may fall back upon a newly developed theory of the pF-curve, which takes into account both the different water binding forces in the soil and the chemical-thermodynamical properties of solid matters and pore solution [2], [3], [9], [10].

The development of structures in CBR-C is not only influenced by the properties of bentonite and by external impacts, but also by the system characteristics arising from the combination of geotextile and bentonite. Thus, the number of fibers per unit area that hold together the upper and lower geotextile layers may be of importance (needling density).

While for the usability of waste dump sealings cyclic moisture impacts excluding frost are the most important factors [4], the slopes of waterways sealed with CBR-C are subjected, among others, to cyclic moisture and frost loading. [5]. The sealing of roadside drainage ditches, on the other hand, are usually provided with thin covers [6], which in the course of a year causes cyclic moisture loading and, in winter time, salt solution and cyclic frost loading. In order to allow for the development of extreme structures, all those loads were included into a one week experimental program.

## 2 EXPERIMENTS AND MATERIAL

### 2.1 *Cyclic experiments*

As the required specimen scale depends on the typical, initially unknown structure dimensions, circular specimens with three different diameters, i.e. d = 5 cm / 11 cm / 30 cm were examined with an identical load of p = 4 kN/m² upon all specimens (Fig. 1).

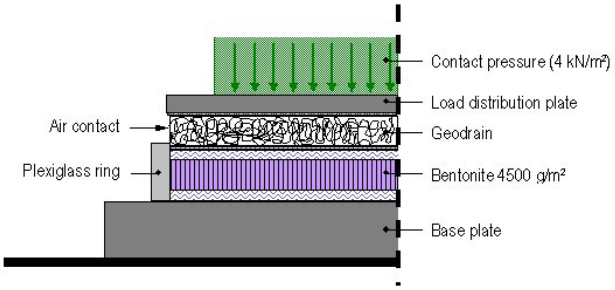


Figure 1 Test setup

Three blocks of tests with a homemade CBR-C and two identical specimens of a commercial product (Table 1) were conducted in parallel. The homemade CBR-C, consisting of two fleeces and completely devoid of any needling, was used for identifying the influence of needling. The two CBR-C specimens of the commercial product were loaded with deionized water and a thawing salt solution, respectively. The test schedule consisted of three cycles of four 12 hours test stages (Fig. 2) which were identical for all specimens:

- Irrigation at room temperature $T_1$ = 22°C,
- Withdrawal of water supply, frost at $T_2$ = -15°C,
- Irrigation at room temperature $T_3$ = 22°C,
- Withdrawal of water supply, stoving at $T_4$ = 40°C.

After the complete experimental programm, the specimens were irrigated for 12 hours at room temperature. Subsequently, water supply was withdrawn. The resultant 9 specimens were deloaded and trapped with light pressure between the base plate and another plastic plate saving them from drying up. Following the first x-ray tomography, the original loaded state was re-established and the specimen was subjected to stoving at 40°C for one week. This was followed by another x-ray tomography which was to identify the differences between the moist and dried up state.

Table 1 Index values of the specimens and the test setup

| Index value | Specimen 1 | Specimen 2 | Specimen 3 |
|---|---|---|---|
| Diameter d [cm] | 5 / 11 / 30 | 5 / 11 / 30 | 5 / 11 / 30 |
| Type | Bentonite between fleeces (Bentonite cf. specim. 2 and 3) | Commercial product, cf. specimen 3 | Commercial product, cf. specimen 2 |
| Mass Bentonite $m_d$ [g/m²] | 4500 | 4500 | 4500 |
| Water | Deionized | Deionized | Thawing salt solution 100 g/l |
| Water supply during irrigation stage | Arbitrary | Arbitrary | Arbitrary |
| Temperatures (Frost / Irrigation / Drying up) | -15 / 22 / 40 | -15 / 22 / 40 | -15 / 22 / 40 |

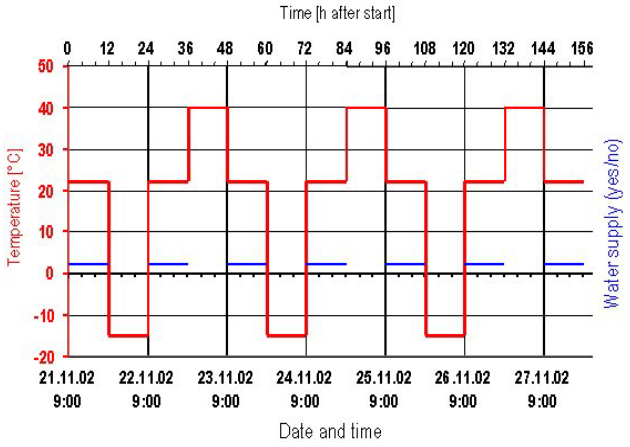


Figure 2 Time-table for the tests with cyclic moisture and temperature loading

## 2.2 *Index values of the bentonite*

In all specimens the same granulated bentonite was used. For the production of specimen 1 this bentonite was taken from a commercial product. The consistency limits as well as further index values were identified (Table 2).

The granulated bentonite showed a significant change when wetted by thawing salt solution in comparison to deionized water. In particular, the swelling behaviour is influenced very strong. This is due to the decreasing thickness of adsorption water layer by increasing salt content and is well known from highly active clays. The swelling of the used granulated bentonite is neglectable at salinity higher than 0,25%, but very intensive at salinity lower than 0,025% (Fig. 3, 4).

Table 2 Index values of the granulated bentonite

| Index value | Lab test or *assumption* |
|---|---|
| Max. grain size $d_{Gmax}$ [mm] (pseudo-grain) | 1.5 |
| Shrinkage limit $w_S$ [%] (Granulate original / Granulate <0.4 mm) | 21.1/ 27.0 |
| Liquid limit $w_L$ [%] (Granulate original / Granulate <0.4 mm) | 481 / 484 |
| Moisture absorption $w_{A,24h}$ [%] (deionized water / thawing salt solution 100g/l) | 112 / 670 |
| Limestone content $V_{Ca}$ [%] | 2.4 |
| Grain density $\rho_S$ [g/cm³] (swelling time 3 days) (Granulate original / Granulate <0,4 mm) | 2.423 / 2.658 |
| pF-curve | *Fig. 5 (Class A prediction)* |
| Clay mineral content in overall mass [%] | 90 |
| Montmorillonite content in clay mineral content [%] | 70 |

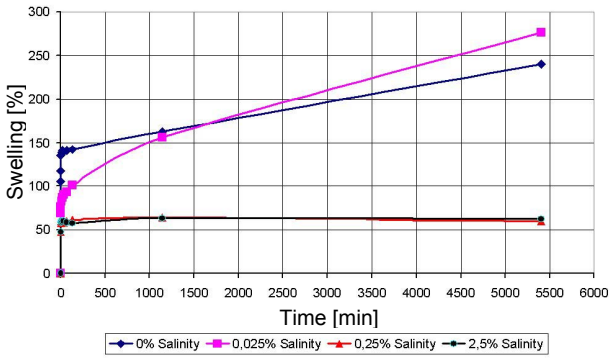


Figure 3 The swelling of bentonite due to the salinity of the moulding-water without surcharge [4]

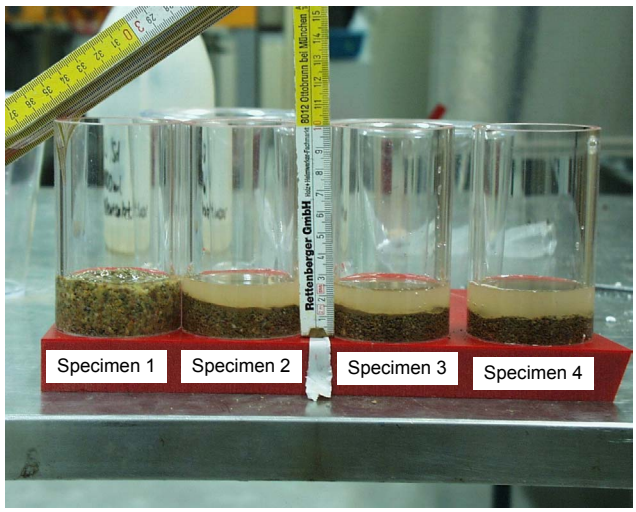


Figure 4 The specimens after swelling for 4 days; specimen 1 is wetted with deionized water (0% salinity) [4]

To the water content $w_S$ at the shrinkage limit corresponds a pore water suction $\psi_S$ at the shrinkage limit, the so-called Air-Entry Value (AEV) (Fig. 5). The calculation equation given in [9], [10] is, however, only applicable to clays with liquid limits smaller than about 70 %. Thus it cannot be applied for bentonite. According to present knowledge, it may be estimated that, depending on the dry density, AEV may

become larger than 100 kN/m² and that it increases in proportion to the homogeneity and density of a specimen, since the air entry is directly determined by the largest pore radii present. The pF-curve, as it may be calculated with the Two-Component-Model [10], is marked by the high adsorbed water content due to the large specific surface.

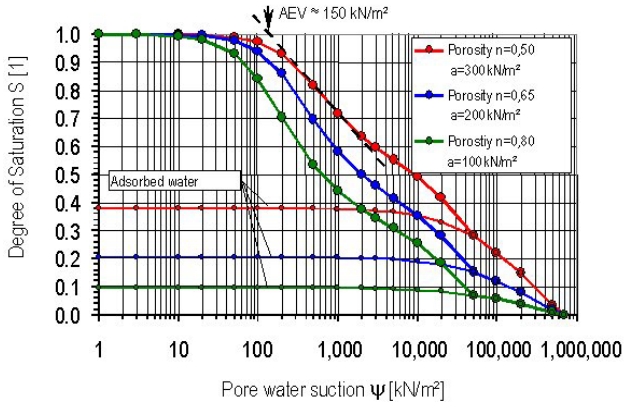


Figure 5 pF-curves of bentonite according to a Class-A-prediction with the Two-Component Model [3], [10] (Model parameter a is about two times AEV and is calculated from liquid and shrinkage limit)

### 2.3 *Shrinkage tests*

In order to identify the temporal development of block sizes and crack intervals in the pure bentonite shrinking after wetting, additional shrinkage tests were conducted on Teflon liner, i.e. with minimized friction.

In the tests both deionized water and thawing salt solution (100g/l) were used. With a mass coating of 4500 g/m² and on a circular surface with d = 30 cm, the bentonite was humidified by spraying, without kneading it.

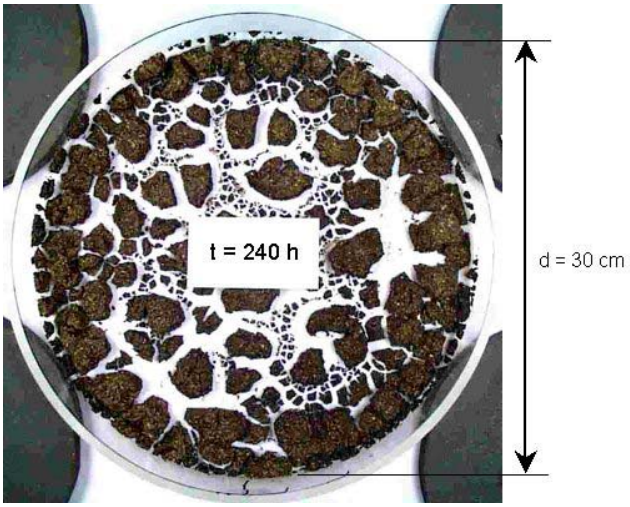


Figure 6 Shrinkage test with d = 30 cm on Teflon liner

The humidification with deionized water resulted in a strong swelling, which led to strong shrinking during the subsequent dehumidification (Fig. 6). As expected the use of thawing salt solution did not result in any swelling. The granule was retained and after the dehumidification was found to be almost as homogeneous as at the start of the test.

Structuring as shown in Fig. 6 may be used for characterizing the bentonite, but – due to the completely different friction and pressure conditions - must not be confused with the actual behavior of the bentonite in practical use, i.e. within the CBR-C. In the test sequence

- shrinkage test (no needling, no friction)
- Test 1 (no needling, geotextile on both sides, friction under mass load)
- Test 2 (needled product, friction under mass load),

the structural dimensions resulting from the cyclic impacts will change from extreme values that are not characteristic of the CBR-C system to possible system values.

## 3 IDENTIFICATION OF STRUCTURES BY MEANS OF X-RAY TOMOGRAPHY

### 3.1 *Implementation and evaluation*

Following the cycle of repeated irrigation at room temperature, followed by freezing or stoving (see Fig. 2), the resultant 9 specimens were examined while humid by means of X-ray topography. The specimens were put into the tomographic unit in a vertical position, which results in a full-circle cross section of the 1 cm thick bentonite layer. Each cross-sectional picture images a thickness of about 1 mm, allowing for multiple cross sections of one and the same layer.

Due to the processing procedures for the production of the specimens and especially due to the structure dimensions resulting from drying, the specimens with their diameter of d = 5 cm are clearly too small for representative analyses. The specimens with d = 11 cm and d = 30 cm did not show any significant differences. However, inhomogeneities were to be found in the larger specimens obviously because of the uneven thickness of the bentonite layer. That limited a uniform evaluation of the pictures. Thus specimens with d = 11 cm are obviously the most suitable specimens for the examination of structuring. That also means that further mass examinations in the lab are facilitated. The following explanations are therefore based on the results of the specimens with a diameter of 11 cm.

The immediate results of X-ray tomographic pictures are gray-scale images that also include information about the density of the structures they show (Fig. 7). The lighter a structure is shown, the larger its mass density. With the help of the evaluation program of the tomographic unit, it is possible to directly state an index value for the density at the position of the mouse cursor (Table 3).

The measured density values show that the dark patterns are practically only filled with air, i.e. that they show real cracks. Contrary to conventional X-ray pictures, the edges are shown more clearly because of the better image resolution. In addition, the thickness of only 1 mm for the cross sections reduces the blurred impression of the block edges resulting from skew running cracks as it may be seen in conventional X-ray pictures through the entire specimen thickness [7].

Table 3 Index values of the mass density of different materials in X-ray tomographic pictures

| Given standard values | | Characteristic values measured in the CBR-C pictures | |
|---|---|---|---|
| Air | -1000 | Plexiglass | +300 |
| Water | 0 | | |
| Bones | +250..+1700 | Light areas ("Blocks") | +800..+1200 |
| Glass | +800 | | |
| Rock, concrete | +1500..+2000 | Dark areas ("Cracks") | -950 |
| Metals | +10000..+18000 | | |

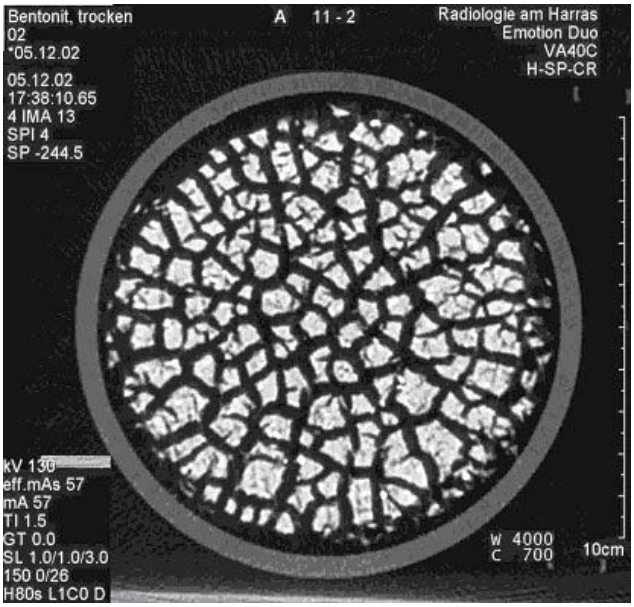


Figure 7 Structuring after loading in accordance with Fig. 2 (specimen 2, diameter d = 11 cm), in dehumidified state (7 days, 40°C in oven, test setup in accordance with Fig. 1)

In order to be able to identify the share of the cracked areas, the gray-scale pictures were converted into 1-bit black-and-white pictures by means of a commercial graphics program. In the process, the gray values still to be converted into black or white are to be selected manually. Settings were made in a way as to apparently give identical dimensions to cracks and blocks. The frequency distribution of the pixel color values then allows to give the percentage of cracked areas (percentage of the black pixels in relation to the overall number of pixels in the picture). For evaluation purposes, a square with a side length of a = 6.5 cm was cut out from the central part of the picture. Thus, only the representative inner face of the pictures was evaluated (Fig. 8, 9, 11).

### 3.2 *Wetted specimens after cyclic loading*

The tomographic examination showed that the specimens were almost intact in a wet condition (Fig. 8). The black, air-filled areas show typical extensions of 0.5 mm. They are point-shaped and have a randomized distribution. No accumulation at possible former crack borders may be discerned.

### 3.3 *Specimens dried in the oven*

Following the above-mentioned examinations, the specimens were again dried in the oven at 40°C and subjected to another, identical X-ray tomographic screening one week later. That examination revealed conspicuous crack patterns (Fig. 7 and Fig. 9 right) which, especially for the completely unneedled specimen 1, resemble the result of the pure shrinkage test (Fig. 9 left).

Compared with the shrinkage test on Teflon liner, the friction conditions at the geotextile clearly influence the homogeneity of the developing structure due to the load of 4 kN/m² (Fig. 9). The blocks and crack widths are clearly smaller and more regular. Nevertheless the friction between the bentonite and the fleece cannot prevent cracks from occurring. This is due to the fact that there is a different stress-strain behavior in the friction between bentonite and geotextile or in the tension load which is induced by shrinking of bentonite. The crack width in the central area of specimen 1 is hardly any larger than at the friction-impacted edges (Fig. 10). This was a typical result of the evaluated cross sections.

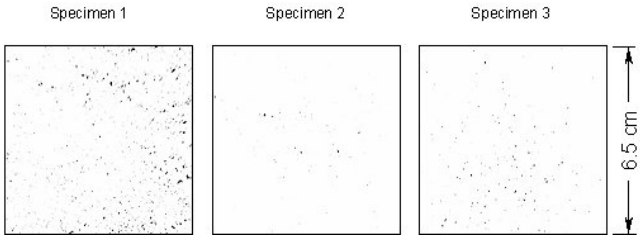


Figure 8 Structuring after loading in accordance with Fig. 2 (specimen diameter d = 11 cm, size of each view 6,5 x 6,5 cm), in humid state

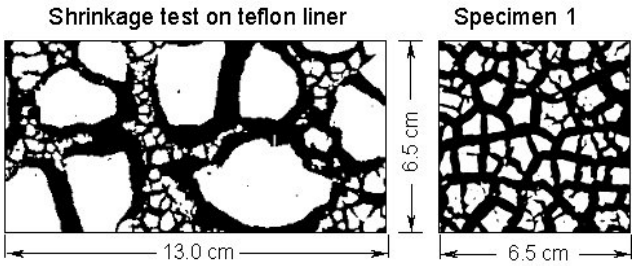


Figure 9 Structuring in specimen 1 after loading in accordance with Fig. 2 and subsequent drying (7 days, 40°C in oven, test setup in accordance with Fig. 1) in comparison with pure shrinkage test (10 days, 22°C)

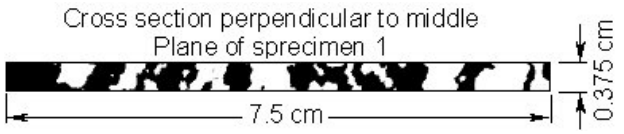


Figure 10 Tomographic cross section perpendicular to middle plane of specimen 1.

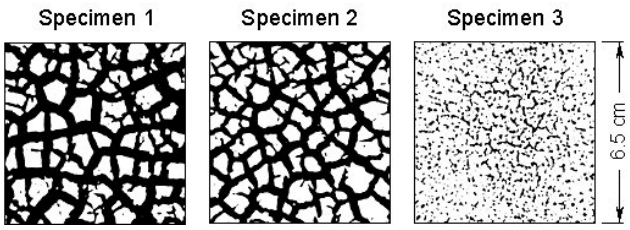


Figure 11 Structuring after loading in accordance with Fig. 2 (specimen diameter d = 11 cm, size of each view 6.5 x 6.5 cm), in dried state (7 days, 40°C in oven, test setup in accordance with Fig. 1)

Needling obviously causes a further reduction of the crack widths (Fig. 11, Comparison of specimens 1 and 2). However, the widths are still rather significant. In specimen 3, which was treated with thawing salt solution, only fine cracks and some scattered flaws may be discerned. That is compliant with the corresponding shrinkage behavior of the pure bentonite (Table 4).

So the main analysis of the test will be possible to make on comparison of structures with and without surface friction, with and without salt solution and with or without needling.

## 4 PARAMETERIZATION OF THE IDENTIFIED STRUCTURES

### 4.1 *Shrinkage test on Teflon liner*

In order to quantify the structures developing in shrinking bentonite layers, the percentages of the cracked area, the crack widths and the surface areas of the blocks were identified.

The largest differences were found between the tests with deionized water and the thawing salt solution, since the latter did not cause any discernable swelling or shrinking.

Deionized water led to very strong swelling and shrinking. The temporal development of those phenomena was photographed and evaluated (Table 4).

After about 10 h the first gaping cracks appeared. The final main crack pattern was complete after about 72 h. Up to then the shrinking process took place with evaporation on only one side. After 120 h, continuous gaping cracks could be observed. The blocks curved up at their edges so that a three-dimensional drying process could take place. The figures in Table 4 refer to later points in time of that test stage.

Table 4 Structure values of the specimen following shrinkage test on Teflon liner (average and extreme values)

| Structure sizes (average values) | | Time t [h] | Deionized water | Thawing salt solution 100 g/l |
|---|---|---|---|---|
| Cracks | Percentage of area [%] | 240<br>336<br>456 | 38.5<br>46.2<br>58.2 | <<1 (points) |
| | Width [mm] Mean (Standard deviation) | 240<br>336<br>456 | 7.7 (5.1)<br>10.8 (5.9)<br>12.5 (6.4) | Not discernible |
| Blocks | Typical area [mm²] of individual blocks, large/small | 240<br>336<br>456 | 908/ 131<br>623/ 85<br>531/ 76 | No blocks discernable |

### 4.2 *Structures in the CBR-C following cyclic loading*

The percentage of cracked areas, the crack width and the surface areas of the blocks were also identified on the basis of the tomographic pictures.

Quantitative analysis was not possible for the specimens treated with the thawing salt solution, since they showed no net pattern of cracks and blocks. The dark areas poor in mass that could be discovered in the pictures rather indicated mostly isolated hollows. With a percentage of cracked areas of about 3 % in a dried state (Fig. 11, right) and < 0.1 % in a still wet state (Fig. 8 right), the bentonite distribution thus stayed obviously very homogeneous.

The influence of the needling gets obvious here in the decrease of the percentage of cracked areas from 56 to 49 % (Table 5, specimens 1 and 2). At the same time the average crack width decreases from 3.4 to 2.2 mm. Once again, we would like to stress that the cyclic loading the specimens are subjected to (Fig. 2) is very strong. Our objective was not to simulate realistic impacts (though we chose a combination of real possible impacts), but to study and describe different types and intensities of structuring. The long-term goal of such studies is also to develop soil-physical structuring models which, for example, model the structures that were identified here due to known loads.

The biggest differences following cyclic loading are to be observed between the still humid state and the dried up state. The percentage of cracked areas increased from 0.1 % to 49 %, cracks with an average width of 2.2 mm appeared. Since the still humid state was almost unharmed after 3 cycles (Table 5), it is to be assumed that the structure recovers well when wetted again. It remains to be evaluated this statement holds true even after a large cycle number or not.

Table 5 Structure values of the CBR-C following cyclic loading in accordance with Fig. 2 (average and extreme values)

| Structure size (average values) | Specimen 1 | Specimen 2 | Specimen 3 |
|---|---|---|---|
| Areas poor mass (cracks): | | | |
| Still humid: area percentage [%] | 0.3 | 0.1 | 0.1 |
| Dry: area percentage [%] | 56 | 49 | 3 |
| Width [mm] Mean (standard deviation) | 3.4 (1.2) | 2.2 (0.8) | approx. 0.5 (point) |
| Areas rich in mass (blocks): | | | |
| Typical area size [mm²] | | | |
| Large | 52 | 69 | No blocks |
| Medium | 31 | 61 | |
| Small | 5 | 6 | |

### 4.3 *Mechanical stability of the shrinkage cracks*

The mechanical stability of vertical cracks in a mineral sealing layer may be estimated by equilibrium of a sliding wedge [10]. For the procedure it does not matter what physical circumstances caused the crack to form (Fig. 12).

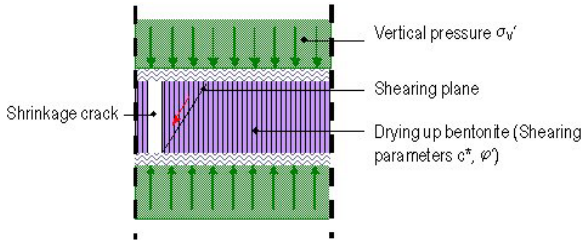


Figure 12 Steadiness of a shrinkage crack in the CBR-C

The load $\sigma'_v$ required for closing the crack depends on the shearing parameters and is as follows:

$$\sigma'_v = 2 \cdot c \cdot \tan\left(45° + \frac{\varphi}{2}\right) \quad (1)$$

Special attention is, however, to be paid to the shearing parameters to be used. What we have on hand is swollen, nearly water-saturated bentonite in an approximately normally consolidated state, which is currently drying up. Even if there once was an apparently preloaded state due to previous drying-wetting cycles, that state will be mostly lost due to the rehumidification because of the high adsorbed water content. An effective cohesion c' therefore does not exist at all or only exists to a very low extent. The effective friction angle for the natrium-activated calcium bentonite is

$\varphi' = 5 .. 10°$ or $\tan \varphi' = 0.087..0.176$.

In the drying state, there are two further strength components that have the effect of cohesion forces: The capillary cohesion $c_k$ as well as the equivalent fiber cohesion $c_f$, if applicable. The latter results from the resistance of the

needling fibers in the direction of the slip joint. While those fibers were, however, already deformed into the opposite direction during the opening of the shrinkage crack, it is assumed here that that portion may approximately be neglected. That leaves for the cohesion c:

$$c = c' + c_f + c_k \approx \psi \cdot \tan\varphi' \qquad \left[\frac{F}{L^2}\right] \tag{2}$$

- with c' ≈ 0 effective cohesion
- $c_f \approx 0$ equivalent fiber cohesion
- $c_k = \psi \cdot \tan\varphi'$ capillary cohesion

Beyond AEV (Fig. 5) the capillary cohesion only increases sublinearly with the soil moisture tension. If we assume $\psi$ to be the soil moisture tension AEV and estimate it to be AEV = 100 kN/m², this results in the vertical tension required for closing the crack:

$$\sigma'_v = 2 \cdot AEV \cdot \tan\varphi' \cdot \tan\left(45° + \frac{\varphi'}{2}\right)$$

$$= 2 \cdot 100 \cdot \tan\varphi' \cdot \tan\left(45° + \frac{\varphi'}{2}\right) \tag{3}$$

$$= 19..42 \frac{kN}{m^2}$$

or a required earth fill height h of about

$$h \approx \frac{\sigma' V}{20} = 1{,}0..2{,}1m \tag{4}$$

Experience has shown that layers with a thickness of about 1.5 m are required for recultivation layers because they act as buffers against temperature and water content changes. Obviously recultivation layers with such thickness also result in a larger probability for the mechanical integrity of CBR-C.

## 5 CONCLUSIONS AND PERSPECTIVE

Significant index values of structured soils may be gathered from X-ray computer tomographic pictures. That is also applicable to clay geosynthetic barriers (CBR-C) which are too sensitive for immediate testing. If CBR-C are opened, the structures may not be retained undisturbed. In such instances test methods avoiding the destruction of structures offer valuable information.

The tests provided structural data (crack widths and crack area percentages, surface area of blocks), which was to be represented by relevant soil-physical models depending on the loads the structures were subjected to. Further studies on that issue ([3], [4], [5]) are under development. There is also a need for further studies on the quality of the involution of structures in a rehumidified state and on the influence of large numbers of cycles in realistic loading. The clarification of those issues will, among others, lead to an improved prognosis concerning the quantities of water flowing through CBR-C. To this end, our Institute also is currently monitoring scientifically some large test fields. [8].

We'd like to thank Dr. med. S. Siuda, Radiologie am Harras, Munich for taking the tomographic pictures of the unusual "patients" and for technical assistance and advice.

## 6 REFERENCES

[1] HEERTEN, G.: Geosynthetic clay liner performance in geotechnical applications. In: Clay Geosynthetic Barriers, Zanzinger, Koerner & Gartung (eds), 2002 Swets & Zeitlinger, Lisse, ISBN 90 5809 380 8

[2] SCHICK, P.: Anwendung eines Zwei-Komponenten-Modells der pF-Kurve auf Strukturänderungen in Böden. Bautechnik 79 (2002), H.2

[3] SCHICK, P.: Die pF-Kurve bindiger Böden bei großen Saugspannungen. Bautechnik 79 (2002), Heft 12, S. 842-849

[4] SCHMITZ, S.: Verhalten von Bentonitmatten unter Frost-Tau-Wechsel. Erster Zwischenbericht, Institut für Bodenmechanik und Grundbau, Universität der Bundeswehr München, 13.12.2002, unpublished

[5] UNOLD, F.: Verhalten von mineralischen Dichtungen bei Frost-Tau-Wechseln. Dritter Zwischenbericht, Institut für Bodenmechanik und Grundbau, Universität der Bundeswehr München, 13.12.2002, unpublished

[6] EGLOFFSTEIN, T.: Der Einfluss des Ionenaustausches auf die Dichtwirkung von Bentonitmatten in Oberflächenabdichtungen von Deponien. ICP Eigenverlag Bauen und Umwelt, Band 3, Karlsruhe 2000

[7] Bundesministerium für Verkehr, Bau- und Wohnungswesen, Abt. Straßenbau, Straßenverkehr (Hrsg.): Geosynthetische Tondichtungsbahnen zum Grundwasserschutz. Forschung Straßenbau und Straßenverkehrstechnik, Heft 848, 2002

[8] SCHMITZ, S. M., SCHULZ, H.: Untersuchungen des Strukturverhaltens von Geosynthetischen Ton-Dichtungsbahnen (zur Veröffentlichung angenommenes Manuskript). In: Handbuch Umweltwissenschaften, ALPHA Verlag, Lampertheim, 2003

[9] SCHICK, P.: The pF-curve of fine-grained soils at high pore water suction. Int. Conf. "From experimental evidence towards numerical modelling of unsaturated soils", ISSMGE, Sept. 18-19, 2003, Bauhaus-University Weimar, Germany, Springer, 2003

[10] SCHICK, P.: A quantitative two-component model of the water binding forces in partially saturated soils (Orig.: Ein quantitatives Zwei-Komponenten-Modell der Porenwasser-Bindekräfte in teilgesättigten Böden). Der Fakultät für Bauingenieur- und Vermessungswesen der Universität der Bundeswehr München vorgelegte Habilitationsschrift, eingereicht am 01.10.2003, noch unveröffentlicht